analytical chemistry

Article

Cite This: *Anal. Chem.* 2018, 90, 9769–9778

pubs.acs.org/ac

Associated Detection of Superoxide Anion and Mercury(II) under Chronic Mercury Exposure in Cells and Mice Models via a Three-Channel Fluorescent Probe

Yue Wang,[†,∥] Min Gao,[†,∥] Qingguo Chen,[§] Fabiao Yu,*[,†,§] Guibin Jiang,[‡] and Lingxin Chen*[,†,§]

[†]CAS Key Laboratory of Coastal Environmental Processes and Ecological Remediation, Research Center for Coastal Environmental Engineering and Technology, Yantai Institute of Coastal Zone Research, Chinese Academy of Sciences, Yantai 264003, China

[‡]State Key Laboratory of Environmental Chemistry and Ecotoxicology, Research Center for Eco-Environmental Sciences, Chinese Academy of Sciences, Beijing 100085, China

[§]School of Marine Science and Technology, Zhejiang Ocean University, Zhoushan 316022, China

[∥]University of Chinese Academy of Sciences, Beijing 100049, China

Supporting Information

ABSTRACT: As a cytotoxic heavy metal ion, mercury(II) ion (Hg^{2+}) induces severe oxidative stress and further results in physiological dysfunction. Although mercury poisoning can be treated with many drugs, such as sodium selenite, the therapeutic effect is relatively poor, and it seems that the damage to human health continues. However, the interpretation for the pathogenesis has not been clarified yet. We supposed that the reason is attributed to Hg^{2+}-caused intracellular oxidative stress. To confirm our hypothesis, we strived to design a three-channel ratio fluorescent probe, HCy−SeH, for superoxide anion ($O_2^{\bullet-}$) and Hg^{2+} combined detection. $O_2^{\bullet-}$ is a vital precursor for other reactive oxygen species (ROS), which is involved in many physiological and pathological processes. However, until now there is no efficient chemical tool for $O_2^{\bullet-}$ and Hg^{2+} combined detection in cells and *in vivo*. The fluorescence response of our probe is initiated by a hydrogen abstraction reaction from the hydrocyanine fluorophore moiety. Once oxidized by $O_2^{\bullet-}$, HCy−SeH recovers its π-conjugated system back to a heptamethine cyanine derivative, Cy−SeH. Cy−SeH coexists with its conjugate base, Cy═Se. One emits red fluorescence, and the other one emits green fluorescence. The response unit, −SeH, can trap Hg^{2+} via a Se−Hg antagonism reaction to afford an orange-emitting final product, Keto−Cy. The probe offers high selectivity and sensitivity toward $O_2^{\bullet-}$ and Hg^{2+}. When applied for $O_2^{\bullet-}$ and Hg^{2+} detection in HEK 293 cells, the imaging results indicate that our probe can provide a combined response for $O_2^{\bullet-}$ and Hg^{2+} in real time and *in situ*. Flow cytometry analysis is well-consistent with the results from fluorescence imaging. When applied to image $O_2^{\bullet-}$ and Hg^{2+} in mice models, we find that Hg^{2+} dominantly accumulates in the kidney and induces a burst of $O_2^{\bullet-}$. We confirm that chronic mercurialism can cause severe oxidative damage and renal fibrosis. HCy−SeH further provides a new information that, even when intracellular Hg^{2+} has been antagonized, the outbreak of $O_2^{\bullet-}$ caused by mercury poisoning still lasts.

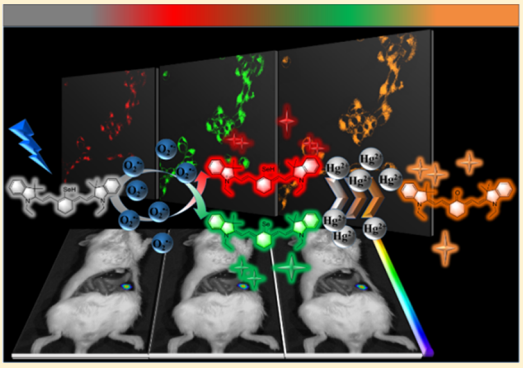

Environmental pollution caused by mercury(II) ion (Hg^{2+}) seriously threatens human health.[1,2] The pollution of Hg^{2+} comes from a variety of ways, such as primary metals production, fossil fuel burning, chemical manufacturing, coal mining, and so on. Hg^{2+} can exist in the environment for a long time. The reason why Hg^{2+} behaves as a fatal heavy metal ion is that it always forms chelates with intracellular electron donors, such as mercapto, carboxyl, carbonyl, and amino. All these groups are expected to play important roles in antioxidant proteins or enzymes. Therefore, mercury poisoning gives rise to many diseases such as central nervous system damage, various cognitive and motor disorders, kidney failure, and even death.[3−5] Studies show that Hg^{2+} can damage many organs, but the kidney suffers the most serious injury.[6] That is, men who are engaged in the mercury-related industry will be inevitably exposed to the mercury-contaminated environment and may suffer from chronic mercury poisoning and other mercury-related diseases. Now many drugs, such as sodium selenite, facilitate the treatment of mercury poisoning. However, the prognosis of therapeutic efficacy is often unsatisfactory. There is much evidence that reveals that Hg^{2+} can be effectively alleviated by many drugs, but its disease symptoms cannot be thoroughly eliminated for a long time. However, the related pathological mechanisms have not yet been clearly elaborated. We suppose that the reason must have

Received: March 30, 2018
Accepted: July 20, 2018
Published: July 20, 2018

DOI: 10.1021/acs.analchem.8b01442
Anal. Chem. 2018, 90, 9769−9778

a close relationship to Hg^{2+}-induced oxidative stress via the damage to the intracellular oxidoreductase.

Superoxide anion ($O_2^{\bullet-}$) is the precursor of other reactive oxygen species (ROS).[7−9] It is an important intermediate in many important physiological and pathological processes. Its intracellular level may reflect the overall concentrations of other ROS. Bodies benefit from a normal level of $O_2^{\bullet-}$. However, the excessive production of $O_2^{\bullet-}$ will result in organism damage, and this allows us to uphold our hypothesis. The mercury-induced burst of $O_2^{\bullet-}$ is available in two ways. One path is that Hg^{2+} induces the lipid peroxide, causing the $O_2^{\bullet-}$ burst.[10] The other path is that Hg^{2+} connects with the mercapto group on the antioxidants such as glutathione and metallothionein, deactivating the antioxidants to induce the overproduction of $O_2^{\bullet-}$.[11,12] $O_2^{\bullet-}$ is involved in many pathological processes,[13,14] such as Parkinson's disease, atherosclerosis, autism, and Alzheimer's disease.[15,16] Thus, the combined detection of intracellular $O_2^{\bullet-}$ and Hg^{2+} changes contributes to understanding their physiological functions and to elucidating the reason for the poor prognosis.

Due to the complex mechanism between $O_2^{\bullet-}$ and Hg^{2+} involved in many physiological and pathological processes, the interaction of $O_2^{\bullet-}$ and Hg^{2+} has become a valuable research area which needs to be further interpreted. There are two major challenges for the associated detection of $O_2^{\bullet-}$ and Hg^{2+}. On the one hand, $O_2^{\bullet-}$ has rapid catabolism properties due to its high reactivity. On the other hand, the sample treatment is too complicated to detect Hg^{2+} *in vivo*. Many technologies have been applied to detect $O_2^{\bullet-}$ or Hg^{2+} separately. For example, the traditional analytical methods for $O_2^{\bullet-}$ detection are usually based on mass spectrometry (MS), electron spin resonance spectroscopy, and high-performance liquid chromatography (HPLC).[17−19] The commonly adopted analytical methods that are used for Hg^{2+} detection are based on atomic absorption spectrometry, atomic emission spectrometry, electron paramagnetic resonance (EPR), and nuclear magnetic resonance (NMR).[20,21] However, these detection methods require complicated sample pretreatment and destruction of tissue or cells. It is difficult to achieve *in situ* and real-time detection in cells and *in vivo*. Additionally, they also cannot realize a combined response of $O_2^{\bullet-}$ and Hg^{2+} during the complicated process. Compared to other biological detection technologies, fluorescence bioimaging technology has powerful potential in the field of bioanalysis because of its high spatial and temporal resolution, good selectivity, excellent sensitivity, less invasiveness, and rapid response.[22−26] So far, fluorescent probes for the detection of $O_2^{\bullet-}$ and Hg^{2+} have been elegantly developed, respectively.[27−39] However, the combined-response fluorescent probe for $O_2^{\bullet-}$ and Hg^{2+} associated detection is urgently required, because the relationship between $O_2^{\bullet-}$ and Hg^{2+} is of great complexity which relates to many diseases. To the best of our knowledge, no fluorescent probe has been developed to date for $O_2^{\bullet-}$ and Hg^{2+} associated detection. For $O_2^{\bullet-}$ and Hg^{2+} combined-response detection, first, we should screen a selective reaction which can avoid interferences coming from other ROS, such as hydroxyl radicals ($^{\bullet}OH$) and hydrogen peroxide (H_2O_2), to detect $O_2^{\bullet-}$ in a complex living system. Second, the group used to detect Hg^{2+} should both specifically respond to Hg^{2+} and avoid interference from other metal ions, such as the physiologically relevant ions Zn^{2+}, Mg^{2+}, and Ca^{2+}. For *in vivo* imaging, the probes whose absorption and emission profiles range in the near-infrared (NIR) region that are able to maximize tissue penetration and to avoid biological background fluorescence will be good candidates for our detection,[40−42] and the ratio signal which employs the ratio of the fluorescence spectra can minimize the interference induced by the uneven loading or the inhomogeneous distribution.[43−47]

Herein, we described a NIR ratiometric three-channel fluorescent probe, HCy−SeH, for the associated detection of $O_2^{\bullet-}$ and Hg^{2+}. HCy−SeH exhibited desirable abilities, such as rapid response time, three-channel fluorescence emission, and high sensitivity, and it could provide a combined response to $O_2^{\bullet-}$ and Hg^{2+} in living cells and *in vivo*. The fluorescence imaging results indicated that Hg^{2+} could induce $O_2^{\bullet-}$ burst in cells. The chronic accumulation of Hg^{2+} would cause severe oxidative stress and lead to cell apoptosis. The results were confirmed by flow cytometry analysis, and cell morphology was investigated by transmission electron microscopy (TEM). Furthermore, HCy−SeH was successfully applied to $O_2^{\bullet-}$ and Hg^{2+} detection in mice models of chronic mercurialism. Importantly, with the help of HCy−SeH, we found that, although the Hg^{2+} could be antagonized by sodium selenite, the overexpressed $O_2^{\bullet-}$ still lasted and caused severe oxidative damage to organisms.

EXPERIMENTAL SECTION

Establishment of the Cell Model of Chronic Mercurialism. Cells were incubated in 25 Petri dishes. When the cells covered 60% of the bottom of the whole dish, different concentrations of Hg^{2+} (groups a, b, c, d, e, and f: 0, 2, 4, 6, 8, and 10 μM, respectively) were added into the dishes for 12 h to establish the chronic mercurialism cell models.

Establishment of the Hg^{2+}-Induced Chronic Mercurialism Mice Models. BALB/c mice weighing about 25−30 g were obtained from Binzhou Medical University. Mice were raised in cages; an SPF laboratory diet and water were acquired freely. Mice were group-housed on a 12:12 light−dark cycle with free access to food and water. To model mice, 18 mg/kg mercury chloride solution was given orally by gavage (0.2 mL) for different days (1, 3, 5, 7, 9, 11 days); the control mice were given equivalent saline. The mice in the treatment group were given sodium selenite 0.5 mg/kg and mercury chloride 18 mg/kg.

Synthesis. Compounds were synthesized according to the general procedure, and characterization details are described in the Supporting Information.

Synthesis of the Probe. Compound **2** (0.12 g, 0.176 mM) was dissolved in 10 mL of EtOH, and then 1.5 equiv of $NaBH_4$ (dissolved in 1 mL of EtOH) was added into the reactive system at 0 °C. After 10 min, the color of the mixture turned to yellow. The mixture was washed with saturated KI solution (bubbled with argon to remove oxygen) for three times and extracted with CH_2Cl_2. The crude product purified with CH_2Cl_2/petroleum ether (1:1 v/v) obtained 0.049 g of yellow solid. Yield: 50%. ^1H NMR (500 MHz, $CDCl_3$-d_1) δ (ppm): 7.18−7.15 (t, 3H), 7.08−7.07 (d, 1H), 6.82−6.79 (t, 2H), 6.65−6.64 (d, 2H), 5.33 (s, 2H), 3.48−3.41(m, 1H), 3.32−3.25 (m, 1H), 2.74−2.64 (m, 2H), 2.59−2.47 (m, 2H), 2.35−2.22 (m, 2H), 1.98 (s, 1H), 1.64−1.62 (d, 6H), 1.47−1.40 (m, 5H), 1.30−1.26 (m, 6H), 1.14−1.11 (t, 3H), 1.07 (m, 3H). ^{13}C NMR (125 MHz, $CDCl_3$-d_1) δ(ppm): 149.37, 139.00, 138.06,130.18,128.64, 127.60, 127.45, 127.23, 126.77, 125.83, 125.72, 125.06, 124.96, 124.09, 123.98, 122.16, 118.67, 108.38, 87.92, 85.35, 53.430, 40.66, 33.512, 31.95, 29.72, 26.49, 25.47,

DOI: 10.1021/acs.analchem.8b01442
Anal. Chem. 2018, 90, 9769−9778

Scheme 1. Molecular Structure and the Proposed Mechanism for $O_2^{\bullet-}$ and Hg^{2+} Associated Detection

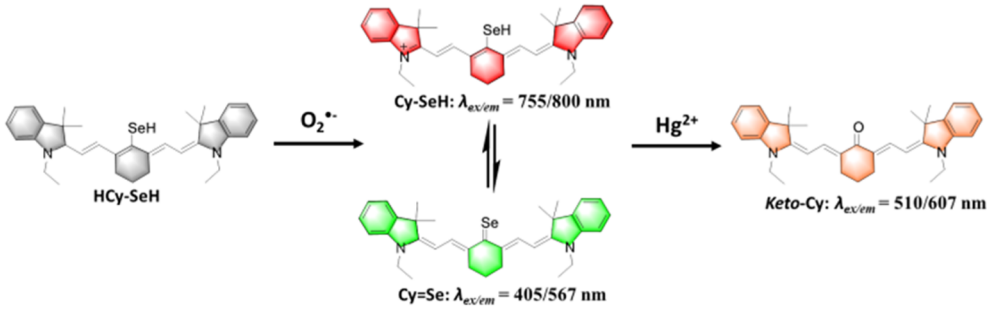

24.36, 22.72, 21.50, 19.33, 15.91, 14.12, 9.97. LC−MS (API-ES): m/z $C_{34}H_{42}N_2Se$; calcd, 558.2513; found $[M - 2H]^+$, 556.2153.

RESULTS AND DISCUSSION

Design Strategy of the Probes. Due to the complexity of $O_2^{\bullet-}$ and Hg^{2+} in the chronic mercury poisoning detection, an efficient tool for $O_2^{\bullet-}$ and Hg^{2+} combined detection is needed urgently. So far as we know, no NIR ratiometric fluorescent probe is used for $O_2^{\bullet-}$ and Hg^{2+} associated detection. Our overall strategy for $O_2^{\bullet-}$ and Hg^{2+} associated response in the biological samples is inspired by two chemical reactions. One is to detect $O_2^{\bullet-}$ through a hydrogen abstraction reaction,[48−50] and the other is to employ a selenium antagonism reaction[51] for Hg^{2+} detection. We choose heptamethine cyanine as the fluorophore because the heptamethine cyanine fluorophore can be reduced for the further detection of $O_2^{\bullet-}$ via hydrogen abstraction reaction (Scheme 1). Moreover, the NIR heptamethine cyanine fluorophore can offer attractive advantages in enlarging tissue penetration and minimizing the absorption of water, myoglobin, hemoglobin, and heme in lipids.[52] We select a selenol (−SeH) group as the response unit because of the strong antagonism effect between inorganic mercury and selenium. As the solubility product constant is lower ($K_{sp\ HgSe} = 10^{-59}$),[53] at least 10 orders of magnitude smaller than that of HgS ($K_{sp\ HgS} = 10^{-47}$), the above reaction is feasible for Hg^{2+} detection in cells, because biothiols, especially glutathione (GSH), concentration is maintained at the millimolar level. We hypothesize that even the Hg^{2+} in the mercury(II)−glutathione complexes can be easily snatched by selenium. That is, the introduction of a −SeH group into the molecular structure of the fluorescent probe will be more selective and sensitive for the detection of Hg^{2+} in cells.[54−59] We masterly integrated −SeH into the middle position of the cyanine platform, and then reduced it with sodium borohydride to afford a probe HCy−SeH (Scheme 1). The synthetic routes of the probe are described in Scheme S1. As illustrated in Scheme 1, our probe exhibited a capability of three-channel response, which could employ the ratio signal and multicolor imaging to realize a multiresponse with a single fluorescent probe.[60] Once the π-electron system of polymethine in cyanine was disturbed by the formation of hydrocyanine, there was no fluorescence emission from HCy−SeH. After the probe HCy−SeH was oxidized by $O_2^{\bullet-}$, Cy−SeH recovered its conjugated system to emit fluorescence. Interestingly, Cy−SeH coexists with its Lewis conjugate base, Cy═Se, in solution. Cy−SeH had red emission with an absorption peak centered at 755 nm and emission peak centered at 800 nm. Cy═Se exhibited green emission with an absorption peak centered at 405 nm and emission peak centered at 567 nm. After being reacted with Hg^{2+}, the final product Keto−Cy formed with a maximum absorption at 510 nm and an emission peak located at 607 nm. HCy−SeH relies on analyte-induced changes in the signal of three emission bands to circumvent inexact complications and greatly improves quantification through an effective internal calibration.[60,61] The common design of the probe has focused on selectivity for individual analytes, but most of the pertinent biological events are related to the interaction of more than one chemical species. It is possible to achieve multiple responses via the simultaneous use of more individual probes. However, the data interpretation will be confounded by the fact that the two separated probes will have different uptake, localization, and emission profiles. An alternative approach is to use a single probe which can respond to two analytes, termed a dual-responsive probe.[62] Our probe, HCy−SeH, is a potential candidate for the associated detection of $O_2^{\bullet-}$ and Hg^{2+}. Hg^{2+} can induce the intracellular $O_2^{\bullet-}$ burst once it invades into the cells. So far, no fluorescent probe can achieve associated detection of $O_2^{\bullet-}$ and Hg^{2+} including a one-channel or two-channel fluorescent probe, and HCy−SeH is the first ratio probe for associated detection of $O_2^{\bullet-}$ and Hg^{2+}. We consider that the three-channel fluorescent probe HCy−SeH will provide excellent detection performance. With the three-channel fluorescent probe HCy−SeH we would obtain more new information about the associated changes of $O_2^{\bullet-}$ and Hg^{2+} in the complicated processes. Spectroscopic properties and selectivity of the probe are displayed in the Supporting Information.

Associated Detection of $O_2^{\bullet-}$ and Hg^{2+} in Chronic Mercurialism Cell Models. Since our probe showed high selectivity and sensitivity for the associated detection of $O_2^{\bullet-}$ and Hg^{2+} in solution, we next assessed the potential utility of the probe for $O_2^{\bullet-}$ and Hg^{2+} detection in complex biological samples. Before cell imaging, we performed an MTT assay to confirm that our probe had low toxicity. The results revealed that our probe showed low cytotoxicity toward cells (Figure S7). Furthermore, the stability and the reaction kinetics of the probe were performed (Figures S2, S3, and S5) to confirm the feasibility of our probe. Then, we used pretreated HEK 293 cells as the cell model. The cells were washed with minimum essential medium (MEM) for three times to remove the additions before imaging. The three-channel images in Figure 1a were constructed via fluorescence collection windows: channel 1 760−850 nm (λ_{ex} = 635 nm), channel 2 λ_{em} = 540−585 nm (λ_{ex} = 405 nm), and channel 3 λ_{em} = 585−685 nm (λ_{ex} = 488 nm). The pseudocolor ratio images were obtained as ratio 1, channel 3 versus channel 2 (the images in channel 2 were collected following by the reaction between the probe

DOI: 10.1021/acs.analchem.8b01442
Anal. Chem. 2018, 90, 9769−9778

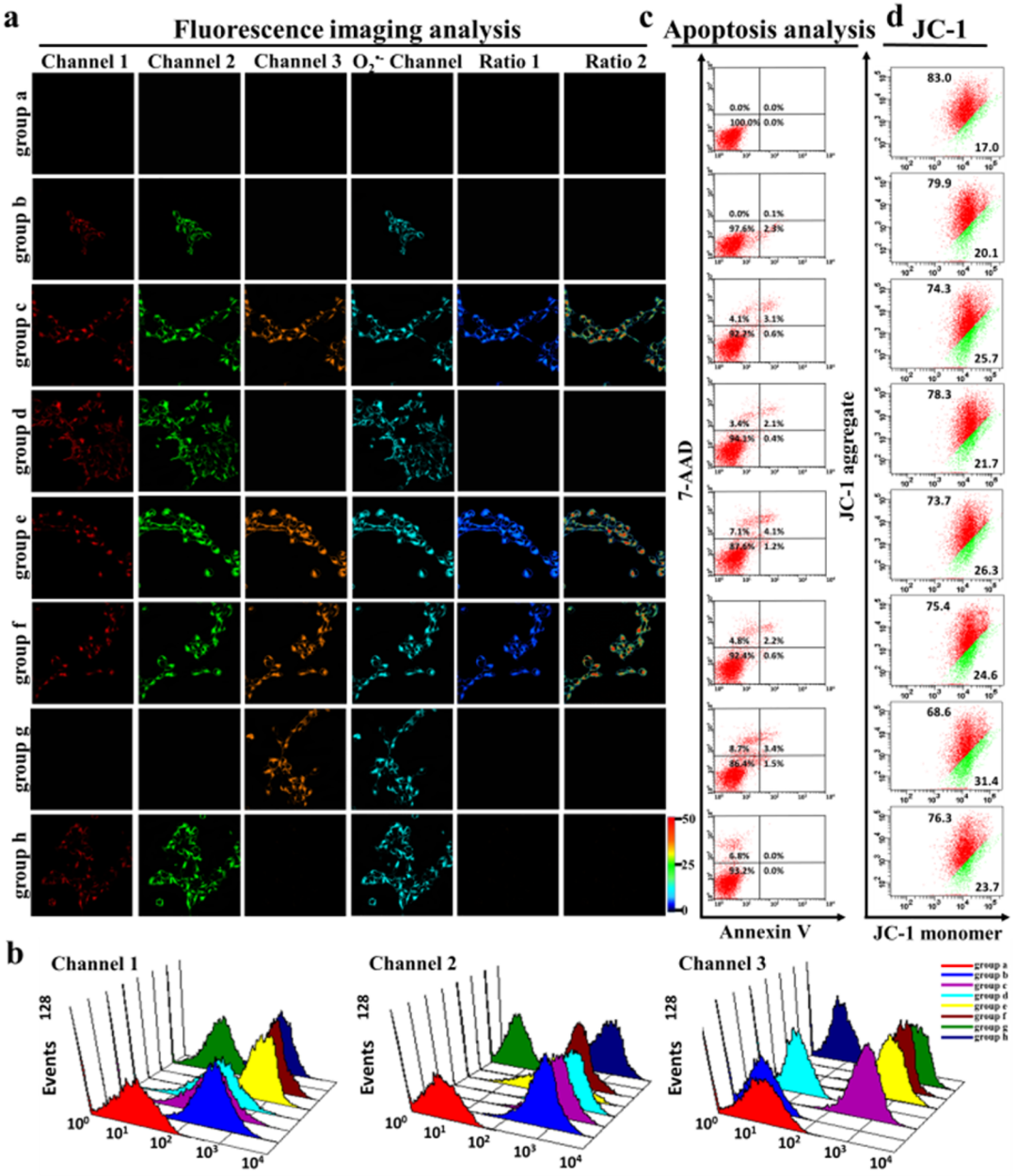

Figure 1. *In situ* detection of $O_2^{\bullet-}$ and Hg^{2+} in HEK 293 cells. (a) Fluorescence imaging of the probe for $O_2^{\bullet-}$ and Hg^{2+} detection by laser scanning confocal microscopy. Channel 1 760−850 nm (λ_{ex} = 635 nm), channel 2 λ_{em} = 540−585 nm (λ_{ex} = 405 nm), channel 3 λ_{em} = 585−685 nm (λ_{ex} = 488 nm), $O_2^{\bullet-}$ channel λ_{em} = 500−530 nm (λ_{ex} = 488 nm); ratio 1, channel 3 vs channel 2; ratio 2, channel 3 vs channel 1. (b) Fluorescence intensity analyzed by flow cytometry. (c) Apoptosis analysis by an Annexin V/7-AAD apoptosis detection kit: viable cells (AnnexinV−/-7-AAD−), early apoptosis (AnnexinV+/7-AAD−), late apoptosis (AnnexinV+/7-AAD+), necrosis (AnnexinV−/7-AAD+). (d) $\Delta\Psi_m$ analysis by JC-1. Group a: The cells were incubated with 10 μM HCy−SeH for 10 min as control. Group b: The cells were pretreated as described in group a, and then $O_2^{\bullet-}$ (10 μM) was added for 15 min. Group c: Then, cells in group c were pretreated as described in group b, and 10 μM Hg^{2+} was added for 15 min. Group d: The cells in group d were pretreated as described in group a, and then stimulated with 10 nM PMA for 20 min. Group e: The cells in group e were manipulated as those in group d, and then 10 μM Hg^{2+} was added for 15 min. Group f: Cells were pretreated as described in group a, and then 10 μM Hg^{2+} was added for 30 min. Group g: Cells were pretreated as described in group a, and then 60 μM Hg^{2+} was added for 30 min. Group h: The cells were pretreated with 30 μM sodium selenite for 60 min, and then the cells were treated as described in group f.

and the Hg^{2+}, and they are shown in the Supporting Information), and ratio 2, channel 3 versus channel 1 (the images in channel 1 were collected following by the reaction between the probe and the Hg^{2+}, and they are shown in the Supporting Information). The commercial ROS fluorescent probe 2,7-dichlorodihydrofluorescein diacetate was used for $O_2^{\bullet-}$ detection. The images were obtained in the $O_2^{\bullet-}$ channel: λ_{em} = 500−530 nm (λ_{ex} = 488 nm). The cells in Figure 1a were divided into eight parallel groups as follows: cells in group a were incubated with HCy−SeH (10 μM) for 10 min as control. All the cells in the other groups were pretreated as described in group a. Cells in group b were incubated with 10 μM $O_2^{\bullet-}$ for 15 min. A fluorescence increase could be observed in channel 1 and channel 2, which was attributed to the π-electron system recovery of the HCy−SeH, and the fluorescence in the $O_2^{\bullet-}$ channel was also

DOI: 10.1021/acs.analchem.8b01442
Anal. Chem. 2018, 90, 9769−9778

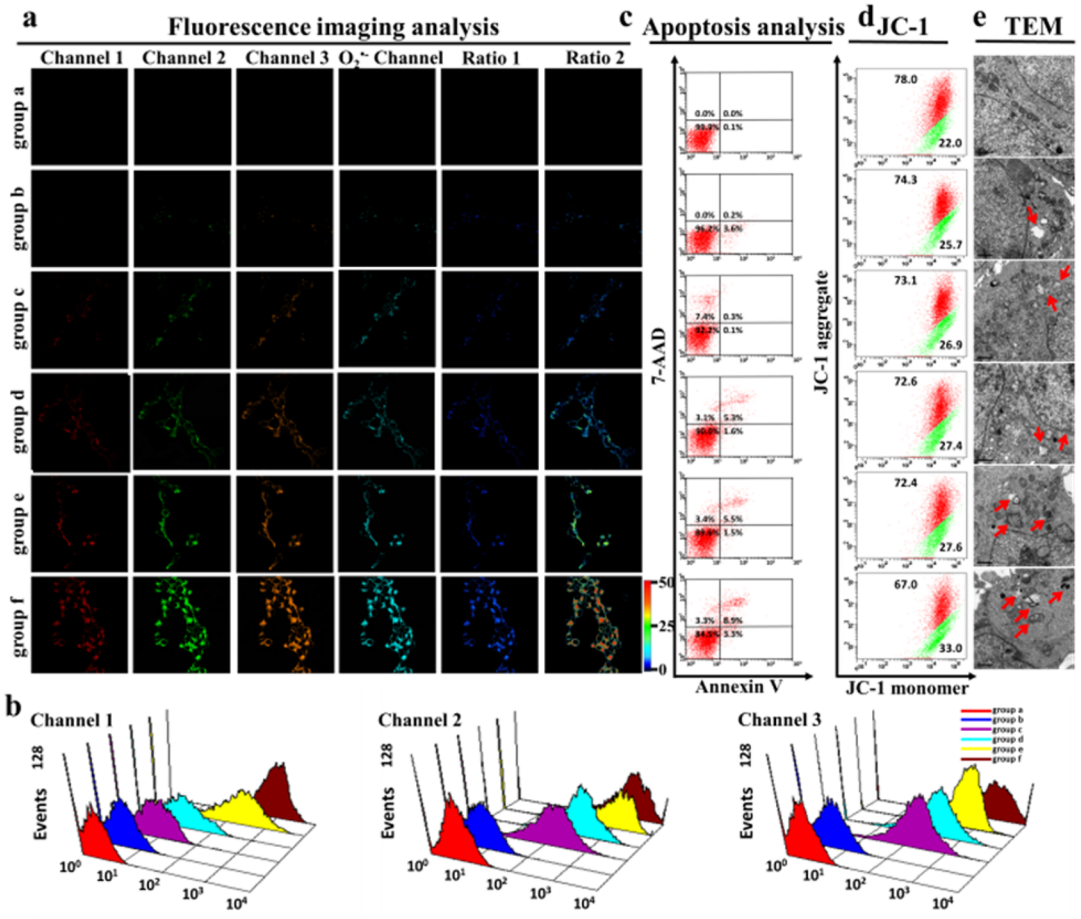

Figure 2. Detection of $O_2^{\bullet-}$ and Hg^{2+} in cells with different concentration of Hg^{2+} stimulation. (a) Laser scanning confocal microscopy analysis. (b) Flow cytometry analysis. (c) Apoptosis analysis by an Annexin V/7-AAD apoptosis detection kit: viable cells (AnnexinV−/7-AAD−), early apoptosis (AnnexinV+/7-AAD−), late apoptosis (AnnexinV+/7-AAD+), necrosis (AnnexinV−/7-AAD+). (d) $\Delta\Psi_m$ analysis by JC-1. (e) TEM observation (scale bars: 1 μm). Concentrations of Hg^{2+}: group a, 0 μM; group b, 2 μM; group c, 4 μM; group d, 6 μM; group e, 8 μM; group f, 10 μM.

obtained. Cells in group c were treated as described in group b, and then incubated with 10 μM Hg^{2+} for 15 min. The vivid fluorescence could be observed in all the three channels. The results demonstrated that our probe, HCy−SeH, could directly associate detect the exogenous $O_2^{\bullet-}$ and Hg^{2+}. Cells in group d were treated as described in group a, and then phorbol myristate acetate (PMA, 10 nM) was added for 20 min to induce endogenous $O_2^{\bullet-}$ generation. The fluorescence signals were collected from channel 1, channel 2, and the $O_2^{\bullet-}$ channel, which indicated the burst of endogenous $O_2^{\bullet-}$. The HEK 293 cells in group e were treated as described in group d, and then 10 μM Hg^{2+} was added. A strong fluorescence enhancement was observed in channel 1, channel 2, channel 3, and the $O_2^{\bullet-}$ channel. As is known to all, Hg^{2+} has cytotoxicity, and it can induce the burst of $O_2^{\bullet-}$ in cells. Cells in group f were incubated with 10 μM Hg^{2+} for 30 min. As expected, strong fluorescence was observed in the three channels as well as the $O_2^{\bullet-}$ channel. The results confirmed that Hg^{2+} could lead to the overproduction of intracellular $O_2^{\bullet-}$. Then, cells in group g were treated with 60 μM Hg^{2+} for 30 min. There was no fluorescence to be collected in channel 1 and channel 2, while channel 3 and the $O_2^{\bullet-}$ channel provided strong fluorescence. The phenomenon was attributed to that Hg^{2+}-induced $O_2^{\bullet-}$ would trigger HCy−SeH to Cy−SeH. However, the high concentration of Hg^{2+} could quickly transform all the probe Cy−SeH to Keto−Cy, and we could not capture the signals in channel 1 and channel 2. Therefore, bright fluorescence was collected only in channel 3 and the $O_2^{\bullet-}$ channel. Sodium selenite has been considered to be a detoxicant for Hg^{2+}; it can protect cells and organisms against the mercury poisoning via selenium−mercury antagonism.[63] Thus, the cells in group h were incubated with 30 μM sodium selenite for 60 min, and then the cells were treated as described in group f. Bright fluorescence images were collected in the channel 1, channel 2, and the $O_2^{\bullet-}$ channel in addition to channel 3. We reasoned that Hg^{2+} could be efficaciously antagonized with selenium. However, Hg^{2+}-induced overproduction of $O_2^{\bullet-}$ lasted, which suggested that cell damage caused by Hg^{2+} was persistent. Cells were difficult to self-repair within a short time, even though mercury antagonist was used. However, sodium selenite terminated the cytotoxicity of Hg^{2+}, and it still played cytoprotective roles in cells. These results confirm our hypothesis at the cellular level. That is, the oxidative stress cause by Hg^{2+} leads to organism damage. Furthermore, flow cytometry analysis has been widely used in cellular quantitative analysis due to its high precision for abundant samples analysis; thus, the fluorescence responses are confirmed by flow cytometry assay (Figure 1b). The results from laser scanning confocal microscopy and flow cytometry were well-consistent, indicating that our probe could be

DOI: 10.1021/acs.analchem.8b01442
Anal. Chem. 2018, 90, 9769−9778

applied for the associated detection of $O_2^{\bullet-}$ and Hg^{2+} in living cells.

The cell apoptosis analysis was performed with an Annexin V/7-AAD apoptosis detection kit (Figure 1c). The apoptosis rates (including necrosis) had been ordered as g (13.6%) > e (12.4%) > c (7.8%) > f (7.6%) > h (6.8%) > d (5.9%) > b (2.4%) > a (0.0%). Compared to the normal cells, cells in the early apoptosis stage have much difference in the mitochondrial membrane potential ($\Delta\Psi_m$). The decreasing red/green fluorescence intensity ratio revealed the increase of cell apoptosis. We utilized the J-aggregate-forming lipophilic cation 5,5′,6,6′-tetrachloro-1,1′,3,3′-tetraethylbenzimidazolylcarbocyanine iodide (JC-1) to further investigate the Hg^{2+}-induced cytotoxicity. As illustrated in Figure 1d, the red/green fluorescence intensity ratio could be ordered as g (68.6%:31.4%) < e (73.7%:26.3%) < c (74.3%:25.7%) < f (75.4%:24.6%) < h (76.3%:23.7%) < d (78.3%:21.7%) < b (79.9%:20.1%) < a (83.0%:17.0%). The results were highly consistent. Our assay revealed that Hg^{2+} had severe cytotoxicity and could cause cell apoptosis and necrosis. The utilization of sodium selenite could rapidly antagonize mercury toxicity in cells, but it could not control the burst of $O_2^{\bullet-}$, which still destroyed the cells with oxidative stress. Therefore, we suggested that, when using reagents to deal with mercury poisoning, we should also pay attention to the control of complication, such as the excessive production of $O_2^{\bullet-}$.

We next established the chronic mercurialism models with HEK 293 cells. The cells were simulated with different concentrations of Hg^{2+} (groups b, c, d, e, and f: 2, 4, 6, 8, and 10 μM, respectively) for 12 h to examine the associated response of $O_2^{\bullet-}$ and Hg^{2+}. Then, the fluorescence images were observed with laser scanning confocal microscopy. As displayed in Figure 2a, the HEK 293 cells in group a were incubated with 10 μM HCy−SeH for 10 min as the control. There was no fluorescence to be observed. With the concentration of Hg^{2+} increased (groups b−f), the four channels, channel 1, channel 2, channel 3, and the $O_2^{\bullet-}$ channel, gradually emitted bright fluorescence. Also, the fluorescence ratio intensity in ratio 1 and ratio 2 increased. The fluorescence changes in the chronic mercurialism models were confirmed by flow cytometry (Figure 2b), and the cell statistical results were well-consistent with those of laser scanning confocal microscopy. These results confirmed that our probe was an efficient chemical tool for the associated detection of $O_2^{\bullet-}$ and Hg^{2+} in cells. Due to the cytotoxicity of Hg^{2+}, we next checked cell apoptosis in these cell models. The apoptosis rates of the cells were assessed employing an Annexin V/7-AAD apoptosis detection kit (Figure 2c) and JC-1 (Figure 2d). In groups a−f, the cell apoptosis rates (including necrosis) were 0.1%, 3.8%, 7.8%, 10.0%, 10.4%, and 15.5%, respectively; the red/green fluorescence intensity ratios in groups a−f were 78.0%:22.0%, 74.3%:25.7%, 73.1%:26.9%, 72.6%:27.4%, 72.4%:27.6%, 67.0%:33.0%. The results of apoptosis analysis demonstrated that the cell apoptosis rate highly depended on the concentrations of Hg^{2+}. The degrees of cell damage were sorted in an order of f > e > d > c > b > a. TEM was used to directly observe the changes of subcellular organelles morphology for evaluating cell damage (Figure 2e). The control cells in group a exhibited continuous and clear nuclear membrane and mitochondria ridge. With the increase of Hg^{2+} the degree of cell injury became severe (groups b−f in Figure 2e). The nuclear membrane and the mitochondrial ridge gradually turned vague, also with mitochondrial swelling, and the density of intracellular cavitation increased. These results further confirmed the cytotoxicity of Hg^{2+}. Our probe, HCy−SeH, was suitable for the associated detection of $O_2^{\bullet-}$ and Hg^{2+} in the chronic mercurialism cell models, and HCy−SeH is potentially exploited as an auxiliary diagnostic tool for the treatment of mercury poisoning. The fluorescence images of the cells in Figure 1 and Figure 2 after the probe reacted with Hg^{2+} are shown in Figures S8 and S10. The bright-field images of Figure 1 and Figure 2 are shown in Figures S9 and S11.

Visualization of $O_2^{\bullet-}$ and Hg^{2+} in Mice. Since the NIR fluorescence can deeply penetrate tissue, protect samples from photodamage, and avoid autofluorescence, we applied our NIR fluorescent probe HCy−SeH for *in vivo* imaging of $O_2^{\bullet-}$ and Hg^{2+}. The *in vivo* imaging assays were performed with an *in vivo* imaging system. The fluorescence images were obtained from three fluorescence collection windows: channel 1 λ_{ex} = 740 nm with filter 790 nm, channel 2 λ_{ex} = 420 nm with filter 570 nm, and channel 3 λ_{ex} = 520 nm with filter 620 nm. The mice in Figure 3a were injected with HCy−SeH (100 μM, 100 μL, in 1:99 DMSO/saline v/v) for 30 min as control. There was no fluorescence to be observed in Figure 3a. The mice in Figure 3b were pretreated with HCy−SeH (100 μM, 100 μL, in 1:99 DMSO/saline, v/v) for 30 min, and then PMA (100 nM, 100 μL in 1:99 DMSO/saline v/v) was injected for 30 min to induce $O_2^{\bullet-}$ generation. The mice in Figure 3b showed clear fluorescence in channel 1 and channel 2. The mice in Figure 3c were preinjected with HCy−SeH (100 μM, 100 μL in 1:99 DMSO/saline v/v), and then Hg^{2+} (30 μM, 100 μL in 1:99 water/saline v/v) was injected for 1 h to induce $O_2^{\bullet-}$ burst. Bright fluorescence was collected in the three channels due to the associated response of $O_2^{\bullet-}$ and Hg^{2+}. These results

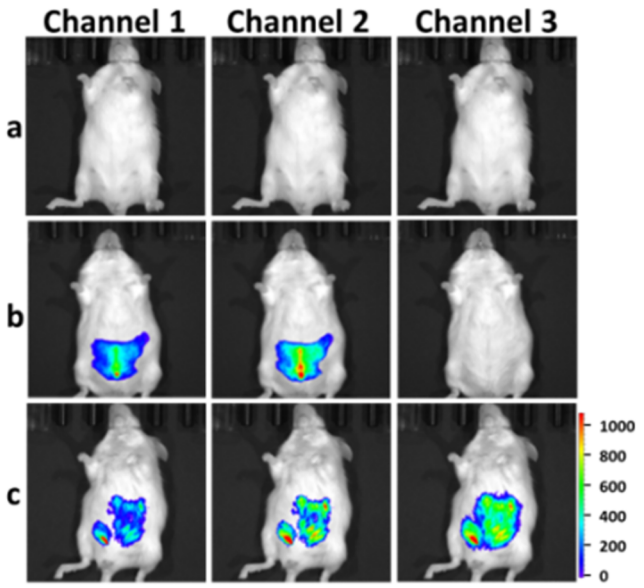

Figure 3. *In vivo* imaging of $O_2^{\bullet-}$ and Hg^{2+} in the peritoneal cavity of mice BALB/c. (a) Mice were ip cavity injected with HCy−SeH (100 μM, 100 μL in 1:99 DMSO/saline v/v) for 30 min. (b) Mice were pretreated with 100 μM HCy−SeH (100 μL in 1:99 DMSO/saline v/v) for 30 min, and then ip injected with PMA (100 nM, 100 μL in 1:99 DMSO/saline v/v) for 30 min. (c) Mice were pretreated as described in panel a, and then the mice were ip cavity injected with Hg^{2+} (30 μM, 100 μL in 1:99 water/saline v/v) for 1 h.

DOI: 10.1021/acs.analchem.8b01442
Anal. Chem. 2018, 90, 9769−9778

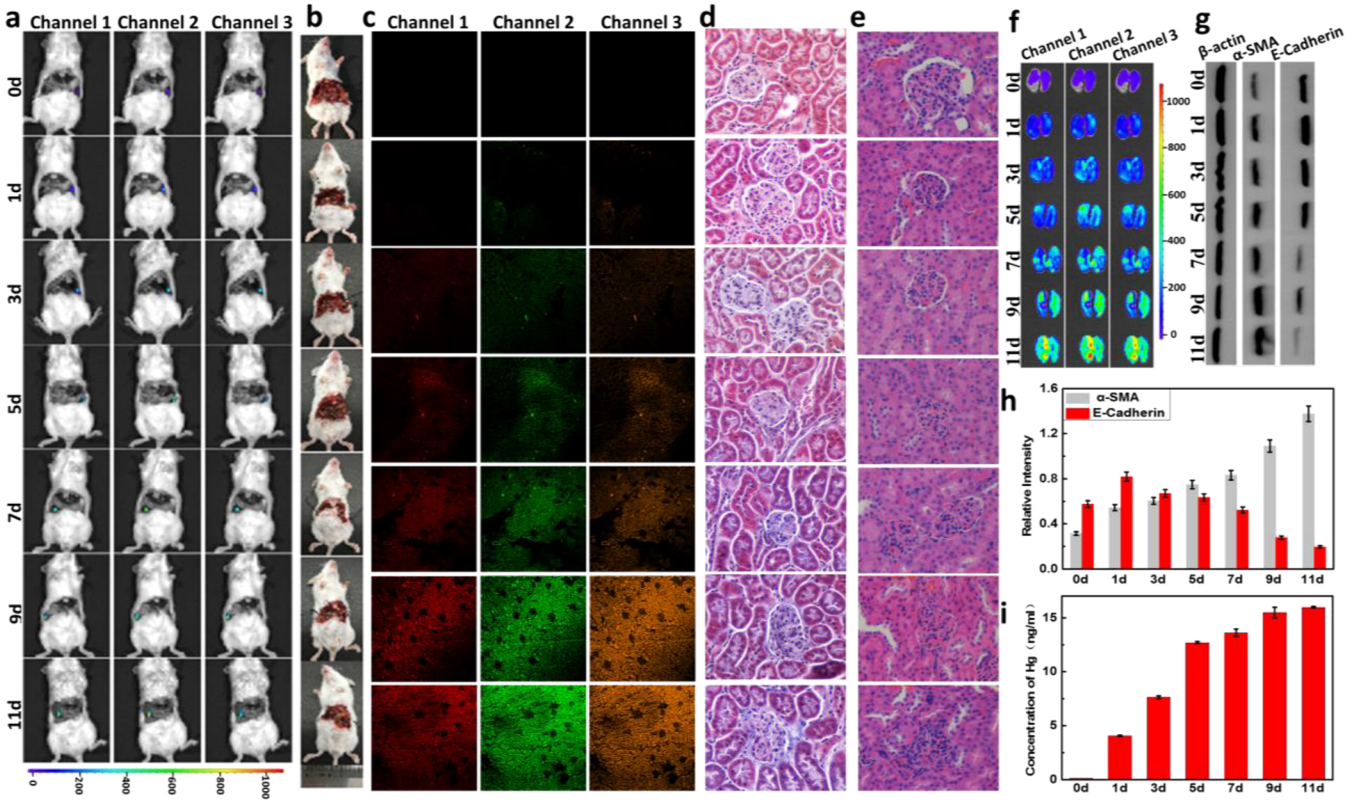

Figure 4. Detection of $O_2^{\bullet-}$ and Hg^{2+} in mice models of chronic mercurialism. (a) Fluorescence imaging of the kidney in the mice of chronic mercurialism through orthotopic injection assay. (b) The details of the organ ligation were obtained from the camera. (c) Fluorescence imaging of the kidney sections. The tissue sections were stained with HCy−SeH (10 μM) for 10 min. (d) Masson's trichrome stain of the kidney sections. (e) H&E staining of the kidney sections from normal and model mice. (f) Fluorescence imaging of the kidneys from the mice in panel a. (g) Western blot analysis of α-SMA and E-cadherin. (h) The relative intensity analysis of α-SMA and E-cadherin by ImageJ software. (i) Detection of Hg^{2+} in kidneys by ICPMS.

demonstrated that the probe HCy−SeH could be used to combine detect $O_2^{\bullet-}$ and Hg^{2+} *in vivo*.

Associated Visualization of $O_2^{\bullet-}$ and Hg^{2+} in the Chronic Mercurialism Mice Models. Among all of the organs, the kidney is the most susceptible organ toward mercury toxicity due to the dominant accumulation of Hg^{2+} in the kidney.[6] Therefore, we try to apply HCy−SeH to the $O_2^{\bullet-}$ and Hg^{2+} associated detection in mice models of chronic mercurialism. The mice models of chronic mercurialism in Figure 4a were given mercury chloride (18 mg/kg in saline/day) orally by gavage with different days (1, 3, 5, 7, 9, 11 days). The mice in group 0 day were given saline orally by gavage as control. The detailed steps are recorded in the Supporting Information. Then, the fluorescence images were obtained with three fluorescence collection windows: channel 1 λ_{ex} = 740 nm with filter 790 nm, channel 2 λ_{ex} = 420 nm with filter 570 nm, and channel 3 λ_{ex} = 520 nm with filter 620 nm. The probe HCy−SeH (10 μM, 10 μL, in 1:99 DMSO/saline v/v) was injected into the kidney through the renal artery for the associated detection of $O_2^{\bullet-}$ and Hg^{2+}. Then, the renal artery and renal vein were ligated as quickly as possible. Finally, with the time extension of mercury stress, the accumulating Hg^{2+} in the kidney would increase the levels of $O_2^{\bullet-}$; thus, the fluorescence signals from channel 1 and channel 2 increased gradually. Furthermore, the fluorescence signals from channel 3 were increasing, indicting the accumulation of Hg^{2+} in kidney (Figure 4a). The kidneys were dissected from chronic mercurialism mice in Figure 4a to acquire the *ex vivo* fluorescence images. As shown in Figure 4f, the increase of fluorescence signals from channel 1 and channel 2 indicated the rising concentrations of $O_2^{\bullet-}$. The fluorescence signals from channel 3 implied that the Hg^{2+} gradually accumulated in the kidney. We also obtained the fresh tissue sections from fresh kidneys for quick detection via fluorescence imaging. As shown in Figure 4c, the changes of fluorescence were consistent with those of Figure 4, parts a and f, and the bright-field images of Figure 4, parts c and f, are shown in Figures S12 and S13.

Chronic mercurialism can cause epithelial−mesenchymal transition (EMT), which is a pathology with a polarized epithelial cell undertaking a mesenchymal cell phenotype through a series of biological processes.[64] The tissue sections of kidney from normal and model mice in Figure 4a were stained by Masson's trichrome stain and H&E (hematoxylin and eosin), respectively. As shown in Figure 4, parts d and e, long-term mercury stress in the kidney could result in EMT, and finally lead to renal interstitial fibrosis. When stained by Masson's trichrome, the collagenous fiber showed in blue color, which was the histological examination for interstitial fibrosis. There were normal collagenous fibers in the control group (Figure 4d), but the collagenous fiber increased gradually along with the days of giving mercury chloride orally by gavage. The pathogenesis was also confirmed by H&E (Figure 4e). The glomerulus of the control group was shown as integral and clear profiles, and the nuclei were regular. However, mercury stress during the 11 days led to an

DOI: 10.1021/acs.analchem.8b01442
Anal. Chem. 2018, 90, 9769−9778

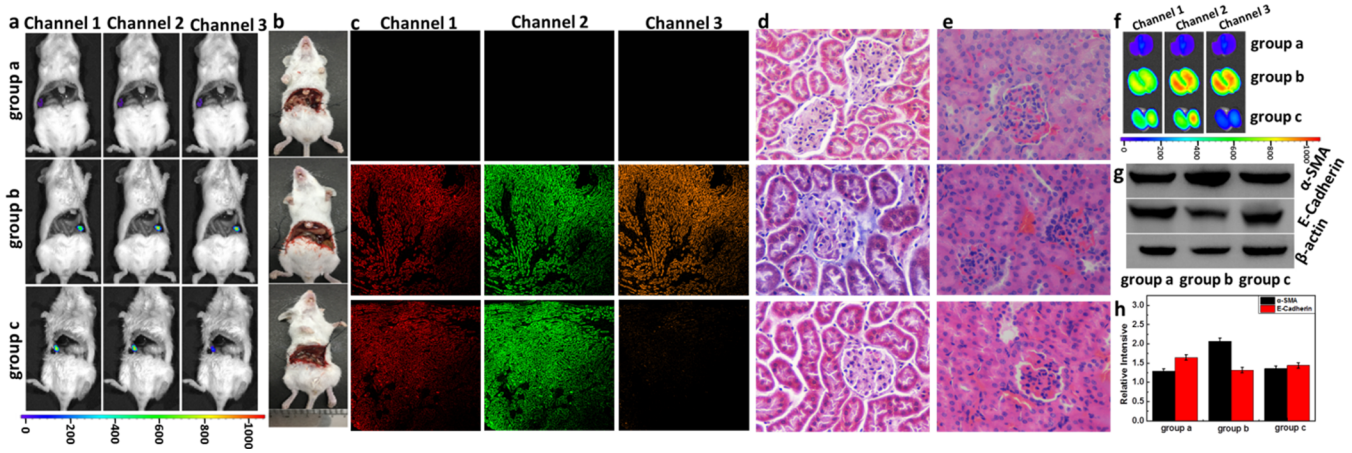

Figure 5. Detection of $O_2^{\bullet-}$ and Hg^{2+} in mice models. (a) Fluorescence imaging of kidneys through orthotopic injection assay. (b) The details of the organ ligation were obtained from the camera. (c) Fluorescence imaging of the kidney sections from normal and model mice. (d) Masson's trichrome stain of the kidney sections from normal and model mice. (e) H&E staining of the kidney sections from the mice in panel a. (f) Fluorescence imaging of the kidneys from the mice in panel a. (g) Western blot analysis of α-SMA and E-cadherin. (h) The relative intensity analysis of α-SMA and E-cadherin by ImageJ software.

incomplete glomerulus profile, which could be attributed to the interstitial fibrosis systemic sclerosis, and then led to the glomerulus distortion. During the EMT process, the level of fibroblast-specific protein α-SMA would increase, and the level of protein E-cadherin which was expressed in epithelial cells would decrease. Due to the kidney damage stimulated by Hg^{2+} primarily in the cortex of the kidney,[65] the protein was extracted from the cortex of the kidney. We performed Western blot assay to investigate the level changes of α-SMA and E-cadherin because the two proteins had been regarded as pathological features of EMT. As shown in Figure 4g, α-SMA was up-regulated and the E-cadherin was down-regulated along with the mercury stress time. It was worth noting that the level of E-cadherin increased. The reason remains to be further studied. The relative quantitative analysis of α-SMA and E-cadherin was determined by the ImageJ software, and the results are shown in Figure 4h. The content of Hg^{2+} in the tissue of the kidney was also determined using inductively coupled plasma mass spectrometry (ICPMS) (Figure 4i). The results demonstrated that Hg^{2+} could accumulate in the kidney. The probe could be used to detect the level of Hg^{2+} in the blood and urine of a mercury poisoning patient. The result was confirmed by atomic absorption spectrometry (AAS, Figure S16).

Sodium selenite had been used as an antagonist for the treatment of mercury poisoning. We next attempted to test the efficacy of sodium selenite on the treatment of chronic mercurialism. The mice in Figure 5a were divided into three groups: The mice in group a were given normal saline (0.2 mL/day) for 11 days as the control. The mice in group b were given mercury chloride (18 mg/kg in 0.2 mL saline) for 11 days as the model group. The mice in group c were given mercury chloride (18 mg/kg) and sodium selenite (0.5 mg/kg) for 11 days as the therapy group. The mice in group a did not show fluorescence (Figure 5, parts a, c, and f). The mice in group b provided bright fluorescence from the three channels, indicating our probe had detected $O_2^{\bullet-}$ and Hg^{2+}. Due to the antagonism between selenium and mercury, only channel 1 and channel 2 gave obvious fluorescence in the mice of group c. Herein, we emphasized that even if mercury chloride and sodium selenite were utilized at the same time, it could also cause a severe burst of $O_2^{\bullet-}$ in the kidney. The bright-field images of Figure 5, parts c and f, are shown in Figures S14 and S15. The fresh tissue sections coming from the mice in groups a–c were stained with Masson's trichrome and H&E, respectively (Figure 5, parts d and e). The images from group a showed the normal morphology of glomeruli, while severe renal fibrosis was observed in group b. The histological sections of the treatment group showed that sodium selenite could well antagonize mercury toxicity. The Western blot was also performed to test the level changes of α-SMA and E-cadherin (Figure 5, parts g and h). In the therapy group, the α-SMA was down-regulated and the E-cadherin was up-regulated compared to the model group. The results also showed the utilization of sodium selenite to treat chronic mercurialism. However, our probe, HCy–SeH, further offered an important information that, although sodium selenite antagonized Hg^{2+}, it could not eliminate the outbreak of $O_2^{\bullet-}$ caused by mercury poisoning. We proposed that the active sites of the intracellular antioxidant system were mainly presented as mercapto or selenol groups. The entrance of Hg^{2+} destroyed the active sites of these enzymes. Even if Hg^{2+} had been antagonized by sodium selenite, it was difficult to recover the antioxidant functions of antioxidant enzymes in a short time. Therefore, we recommend that one should pay attention to the damage caused by oxidative stress during the treatment of mercury poisoning.

CONCLUSION

In conclusion, to confirm the proposed mechanism that the oxidative stress cause by Hg^{2+} leads to poor prognosis of the mercury poisoning, we designed and synthesized a NIR three-channel fluorescent probe, HCy–SeH, for the associated detection of $O_2^{\bullet-}$ and Hg^{2+} in cells and mice models of chronic mercury poisoning. When used for the detection, the three-channel responses provided ratio fluorescence signals which can eliminate the interference induced by the uneven loading or the inhomogeneous distribution. The probe exhibits high selectivity and sensitivity toward the associated detection of $O_2^{\bullet-}$ and Hg^{2+}. The fluorescence imaging and the flow cytometry analysis demonstrate that the probe can be used to *in situ* detect $O_2^{\bullet-}$ and Hg^{2+} in HEK 293 cell models. The

DOI: 10.1021/acs.analchem.8b01442
Anal. Chem. 2018, 90, 9769–9778

results demonstrate that the accumulation of Hg^{2+} will interrupt the cellular antioxidant system and induce the overproduction of $O_2^{\bullet-}$. We successfully applied the probe to the utilization in mice models of chronic mercurialism. The results confirm that mercury poisoning can cause kidney damage and lead to renal fibrosis. We employed sodium selenite to antagonize Hg^{2+} *in vivo*. Although this antagonist can efficaciously relieve the chronic mercurialism, it cannot reduce the high level of $O_2^{\bullet-}$. Therefore, the organism damage caused by Hg^{2+} may continue in a long term. These results highlight that our probe can be used as a powerful tool for $O_2^{\bullet-}$ and Hg^{2+} associated detection *in vitro* and *in vivo*. We believe that our probe can be a benefit for clinical surgery pre-evaluation.

■ ASSOCIATED CONTENT

Supporting Information

The Supporting Information is available free of charge on the ACS Publications website at DOI: 10.1021/acs.analchem.8b01442.

More experimental materials and details, synthesis steps, and characterization of compounds (PDF)

■ AUTHOR INFORMATION

Corresponding Authors

*E-mail: fbyu@yic.ac.cn.

*E-mail: lxchen@yic.ac.cn.

ORCID

Fabiao Yu: 0000-0003-0073-6299

Lingxin Chen: 0000-0002-3764-3515

Notes

The authors declare no competing financial interest.

■ ACKNOWLEDGMENTS

We thank the National Nature Science Foundation of China (nos. 21575159, 21775162, 41776110, 41506126, and 21405172), the program of Youth Innovation Promotion Association, CAS (Grant 2015170), the Instrument Developing Project of the Chinese Academy of Sciences (YZ201662), and the Key Laboratory of Sensor Analysis of Tumor Marker, Ministry of Education, Qingdao University of Science and Technology (Grant SATM201705).

■ REFERENCES

(1) Chen, X.; Pradhan, T.; Wang, F.; Kim, J. S.; Yoon, J. *Chem. Rev.* **2012**, *112*, 1910−1956.

(2) Bera, K.; Das, A. K.; Nag, M.; Basak, S. *Anal. Chem.* **2014**, *86*, 2740−2746.

(3) Du, J.; Fan, J.; Peng, X.; Sun, P.; Wang, J.; Li, H.; Sun, S. *Org. Lett.* **2010**, *12*, 476−479.

(4) Jiang, J.; Liu, W.; Cheng, J.; Yang, L.; Jiang, H.; Bai, D.; Liu, W. *Chem. Commun.* **2012**, *48*, 8371−8373.

(5) Ko, S. K.; Yang, Y. K.; Tae, J.; Shin, I. *J. Am. Chem. Soc.* **2006**, *128*, 14150−14155.

(6) Sin, Y. M.; Lim, Y. F.; Wong, M. K. B. *Bull. Environ. Contam. Toxicol.* **1983**, *31*, 605−612.

(7) Zhang, W.; Li, P.; Yang, F.; Hu, X.; Sun, C.; Zhang, W.; Chen, D.; Tang, B. *J. Am. Chem. Soc.* **2013**, *135*, 14956.

(8) Dickinson, B. C.; Chang, C. J. *Nat. Chem. Biol.* **2011**, *7*, 504.

(9) Chen, X.; Tian, X.; Shin, I.; Yoon. *Chem. Soc. Rev.* **2011**, *40*, 4783−4804.

(10) Stacchiotti, A.; Morandini, F.; Bettoni, F.; Schena, I.; Lavazza, A.; Grigolato, P. G.; Apostoli, P.; Rezzani, R.; Aleo, M. F. *Toxicology* **2009**, *264*, 215−224.

(11) Hayes, J. D.; Flanagan, J. U.; Jowsey, I. R. *Annu. Rev. Pharmacol. Toxicol.* **2005**, *45*, 51−88.

(12) Goering, P. L.; Morgan, D. L.; Ali, S. F. J. *J. Appl. Toxicol.* **2002**, *22*, 167−172.

(13) Winterbourn, C. C. *Nat. Chem. Biol.* **2008**, *4*, 278.

(14) Brownlee, M. *Nature* **2001**, *414*, 813.

(15) Cai, H.; Harrison, D. G. *Circ. Res.* **2000**, *87*, 840.

(16) Mattson, M. P. *Nature* **2004**, *430*, 631.

(17) Zhang, J.; Li, C.; Zhang, R.; Zhang, F.; Liu, W.; Liu, X.; Lee, S. M. Y.; Zhang, H. *Chem. Commun.* **2016**, *52*, 2679.

(18) Nilsson, U. A.; Haraldsson, G.; Bratell, S.; Sorensen, V.; Akerlund, S.; Pettersson, S.; Schersten, T.; Jonsson, O. *Acta Physiol. Scand.* **1993**, *147*, 263−270.

(19) Gao, X.; Feng, G.; Manghnani, P. N.; Hu, F.; Jiang, N.; Liu, J.; Liu, B.; Sun, J. Z.; Tang, B. Z. *Chem. Commun.* **2017**, *53*, 1653−1656.

(20) dos Santos, J. S.; de la Guardia, M.; Pastor, A.; dos Santos, M. L. P. *Talanta* **2009**, *80*, 207−211.

(21) Feng, L.; Chen, Z. *Sens. Actuators, B* **2007**, *122*, 600−604.

(22) Gao, M.; Yu, F.; Chen, H.; Chen, L. *Anal. Chem.* **2015**, *87*, 3631−3638.

(23) Han, X.; Yu, F.; Song, X.; Chen, L. *Chem. Sci.* **2016**, *7*, 5098−5107.

(24) Xu, Z.; Baek, K. H.; Kim, H. N.; Cui, J.; Qian, X.; Spring, D. R.; Shin, I.; Yoon, J. *J. Am. Chem. Soc.* **2010**, *132*, 601−610.

(25) Xu, Z.; Singh, N. J.; Lim, J.; Pan, J.; Kim, H. N.; Park, S.; Kim, K. S.; Yoon, J. *J. Am. Chem. Soc.* **2009**, *131*, 15528.

(26) Gao, M.; Yu, F.; Lv, C.; Choo, J.; Chen, L. *Chem. Soc. Rev.* **2017**, *46*, 2237−2271.

(27) Hu, J. J.; Wong, N. K.; Ye, S.; Chen, X.; Lu, M. Y.; Zhao, A. Q.; Guo, Y.; Ma, A. C. H.; Leung, A. Y. H.; Shen, J.; Yang, D. *J. Am. Chem. Soc.* **2015**, *137*, 6837−6843.

(28) Lu, D.; Zhou, L.; Wang, R.; Zhang, X. B.; He, L.; Zhang, J.; Hu, X.; Tan, W. *Sens. Actuators, B* **2017**, *250*, 259−266.

(29) Li, R. Q.; Mao, Z. Q.; Rong, L.; Wu, N.; Lei, Q.; Zhu, J. Y.; Zhuang, L.; Zhang, X. Z.; Liu, Z. H. *Biosens. Bioelectron.* **2017**, *87*, 73−80.

(30) Li, P.; Zhang, W.; Li, K.; Liu, X.; Xiao, H.; Zhang, W.; Tang, B. *Anal. Chem.* **2013**, *85*, 9877−9881.

(31) Chen, X.; Wang, F.; Hyun, J. Y.; Wei, T.; Qiang, J.; Ren, X.; Shin, I.; Yoon, J. *Chem. Soc. Rev.* **2016**, *45*, 2976.

(32) Ding, J.; Li, H.; Wang, C.; Yang, J.; Xie, Y.; Peng, Q.; Li, Q.; Li, Z. *ACS Appl. Mater. Interfaces* **2015**, *7*, 11369−11376.

(33) Song, C.; Yang, W.; Zhou, N.; Qian, R.; Zhang, Y.; Lou, K.; Wang, R.; Wang, W. *Chem. Commun.* **2015**, *51*, 4443.

(34) Zhang, X.; Xiao, Y.; Qian, X. *Angew. Chem., Int. Ed.* **2008**, *47*, 8025−8029.

(35) Hu, B.; Hu, L. L.; Chen, M. L.; Wang, J. H. *Biosens. Bioelectron.* **2013**, *49*, 499−505.

(36) Gong, Y. J.; Zhang, X. B.; Zhang, C. C.; Luo, A. L.; Fu, T.; Tan, W.; Shen, G. L.; Yu, R. Q. *Anal. Chem.* **2012**, *84*, 10777−10784.

(37) Ando, S.; Koide, K. *J. Am. Chem. Soc.* **2011**, *133*, 2556.

(38) Song, F.; Watanabe, S.; Floreancig, P. E.; Koide, K. *J. Am. Chem. Soc.* **2008**, *130*, 16460−16461.

(39) Diaz de Grenu, B.; Garcia Calvo, J.; Cuevas, J.; Garcia Herbosa, G.; Garcia, B.; Busto, N.; Ibeas, S.; Torroba, T.; Torroba, B.; Herrera, A.; Pons, S. *Chem. Sci.* **2015**, *6*, 3757−3764.

(40) Li, L.; Li, Z.; Shi, W.; Li, X.; Ma, H. *Anal. Chem.* **2014**, *86*, 6115−6120.

(41) Gong, Y. J.; Zhang, X. B.; Mao, G. J.; Su, L.; Meng, H. M.; Tan, W.; Feng, S.; Zhang, G. *Chem. Sci.* **2016**, *7*, 2275−2285.

(42) Yuan, L.; Lin, W.; Zheng, K.; He, L.; Huang, W. *Chem. Soc. Rev.* **2013**, *42*, 622−661.

(43) Zhao, C.; Zhang, X.; Li, K.; Zhu, S.; Guo, Z.; Zhang, L.; Wang, F.; Fei, Q.; Luo, S.; Shi, P.; Tian, H.; Zhu, W. H. *J. Am. Chem. Soc.* **2015**, *137*, 8490−8498.

DOI: 10.1021/acs.analchem.8b01442
Anal. Chem. 2018, 90, 9769−9778

(44) Yuan, L.; Lin, W.; Yang, Y. *Chem. Commun.* **2011**, *47*, 6275−6277.
(45) Fan, J.; Sun, W.; Hu, M.; Cao, J.; Cheng, G.; Dong, H.; Song, K.; Liu, Y.; Sun, S.; Peng, X. *Chem. Commun.* **2012**, *48*, 8117−8119.
(46) Yu, F.; Li, P.; Song, P.; Wang, B.; Zhao, J.; Han, K. *Chem. Commun.* **2012**, *48*, 2852−2854.
(47) Ueno, T.; Nagano, T. *Nat. Methods* **2011**, *8*, 642.
(48) Yu, F.; Gao, M.; Li, M.; Chen, L. *Biomaterials* **2015**, *63*, 93−101.
(49) Lebel, C. P.; Ischiropoulos, H.; Bondy, S. C. *Chem. Res. Toxicol.* **1992**, *5*, 227−231.
(50) Buxser, S. E.; Sawada, G.; Raub, T. J. *Methods Enzymol.* **1999**, *300*, 256−275.
(51) Khan, M. A. K.; Wang, F. *Environ. Toxicol. Chem.* **2009**, *28*, 1567−1577.
(52) Han, X.; Song, X.; Yu, F.; Chen, L. *Adv. Funct. Mater.* **2017**, *27*, 1700769.
(53) Hankare, P. P.; Bhuse, V. M.; Garadkar, K. M.; Delekar, S. D.; Mulla, I. S. *Semicond. Sci. Technol.* **2004**, *19*, 70.
(54) Kim, H. N.; Ren, W. X.; Kim, J. S.; Yoon, J. *Chem. Soc. Rev.* **2012**, *41*, 3210−3244.
(55) Shi, W.; Sun, S.; Li, X.; Ma, H. *Inorg. Chem.* **2010**, *49*, 1206−1210.
(56) Tang, B.; Ding, B.; Xu, K.; Tong, L. *Chem. - Eur. J.* **2009**, *15*, 3147−3151.
(57) Samb, I.; Bell, J.; Toullec, P. Y.; Michelet, V.; Leray, I. *Org. Lett.* **2011**, *13*, 1182−1185.
(58) Kumar, A.; Singh, J. D. *Inorg. Chem.* **2012**, *51*, 772.
(59) Li, Y.; He, S.; Lu, Y.; Zeng, X. *Org. Biomol. Chem.* **2011**, *9*, 2606−2609.
(60) Zhang, Q.; Zhu, Z.; Zheng, Y.; Cheng, J.; Zhang, N.; Long, Y. T.; Zheng, J.; Qian, X.; Yang, Y. *J. Am. Chem. Soc.* **2012**, *134*, 18479−18482.
(61) Lee, M. H.; Kim, J. S.; Sessler, J. L. *Chem. Soc. Rev.* **2015**, *44*, 4185−4191.
(62) Kolanowski, J. L.; Liu, F.; New, E. J. *Chem. Soc. Rev.* **2018**, *47*, 195−208.
(63) Pelletier, E. *Mar. Environ. Res.* **1986**, *18*, 111−132.
(64) Kalluri, R.; Weinberg, R. A. J. *J. Clin. Invest.* **2009**, *119*, 1420−1428.
(65) Goering, P. L.; Fisher, B. R.; Noren, B. T.; Papaconstantinou, A.; Rojko, J. L.; Marler, R. J. *Toxicol. Sci.* **2000**, *53*, 447−457.

DOI: 10.1021/acs.analchem.8b01442
Anal. Chem. 2018, 90, 9769−9778